3-D MHD model of the Sun-solar wind system : The first results

Nakamizo, Aoi
Department of Earth and Planetary Sciences, Faculty of Sciences, Kyushu University | CREST, Japan Science and Technology Agency

Tanaka, Takashi
Department of Earth and Planetary Sciences, Faculty of Sciences, Kyushu University | CREST, Japan Science and Technology Agency

Kamei, Satomi
Department of Earth and Planetary Sciences, Graduated School of Sciences, Kyushu University | CREST, Japan Science and Technology Agency

Shimazu, Hironori
National Institute of Information and Communications | CREST, Japan Science and Technology Agency

他

https://doi.org/10.5109/13528

出版情報：九州大学大学院理学研究院紀要 : Series D, Earth and planetary sciences. 32 (2), pp.69-86, 2009-03-02. Faculty of Science, Kyushu University
バージョン：
権利関係：

Mem. Fac. Sci., Kyushu Univ., Ser. D, Earth & Planet. Sci., Vol. XXXII, No. 2,
pp. 69-86, March 2, 2009

3-D MHD model of the Sun-solar wind system: The first results

Aoi Nakamizo[*,****], Takashi Tanaka[*,****], Satomi Kamei[**,****], Hironori Shimazu[***,****] and Hiroyuki Shinagawa[***,****]

Abstract

Toward the integrated numerical space weather prediction, we have been developing a three dimensional MHD simulation model of the sun-solar wind combining system. Here we describe the overview of the model and report on the first result of the simulation. Appling the unstructured grid system, we achieved the dense grid spacing at the inner boundary, which enable us to treat the fine structure near the sun, and a size of simulation space of 1AU, simultaneously. The magnetic field at the inner boundary is prescribed with the observational data of photospheric magnetic field during a specific time period. In order to obtain the supersonic solar wind, the parametric source functions are introduced into the energy equation and momentum equation. The source functions are in the exponentially dumping form as has been widely used in previous works. However the intensities of the source functions are newly adjusted so as to reflect the topology of the coronal magnetic field. They are increased inside the magnetic flux tube in sub-radial expansion and reduced inside the magnetic flux tube in over-radial expansion. This adjustment aims to reproduce the variation of the solar wind speed according to the coronal magnetic field. It is confirmed from the data comparison that the MHD model successfully reproduced many features both of the solar coronal region and the solar wind 3-D structure. With the further improvement and refinement, the model will be applied to the integrated space weather simulation system being developed at NiCT (National institute of Information and Communication Technology), Japan.

Keywords: solar wind, MHD simulation, expansion factor, space weather

1. Introduction

The solar wind is one of the primary factors controlling the terrestrial environment. Also the underlying structure of the solar wind partly determines the propagation of solar disturbance phenomena, such as coronal mass ejections (CMEs) or high-energy particles associated with solar flares, which occasionally cause serious effects on the terrestrial environment. Therefore it cannot be

Manuscript received on 4 September 2008; accepted on 27 November 2008
* Department of Earth and Planetary Sciences, Faculty of Sciences, Kyushu University, Higashi-ku, Fukuoka 812-8581, JAPAN; aoi@geo.kyushu-u.ac.jp
** Department of Earth and Planetary Sciences, Graduated School of Sciences, Kyushu University, Higashi-ku, Fukuoka 812-8581, JAPAN
*** National Institute of Information and Communications Technology, 4-2-1, Koganei-shi, Tokyo 184-8795, JAPAN
**** CREST, Japan Science and Technology Agency, Kawaguchi-shi, Saitama 332-0012, JAPAN

overemphasized that the learning the structure of the solar wind from its source region to the earth's orbit and beyond is the important part of the study of the solar-terrestrial physics.

The overall picture of the interplanetary space have been obtained by a number of observations including the discovery of the recurrent structure made by Mariner 10 (Ness and Wilcox, 1965) and the latitudinal structure revealed by Ulysses (Phillips et al., 1995; McComas et al., 1998; McComas et al., 2002). During solar minimum, the interplanetary space is highly structured under the solar magnetic field which is close to the dipole field: fast tenuous wind in higher latitudes and slow dense wind near the equator with the sharp transition in between (Phillips et al., 1995; McComas et al., 1998). The fast wind is generally believed to be originated with large polar coronal holes. The slow wind is thought to be associated with streamers near the equator, boundaries between closed and open magnetic field and so on, although its origin is not precisely determined. The first WSM (Whole Sun Month) campaign conducted from August 10 to September 8, 1996, which was close to the solar minimum, further promoted the above picture (e.g., Neugebauer et al., 1998; Linker et al., 1999). While during solar maximum the interplanetary space departs from the structured one (e.g., McComas et al., 2002; Neugebauer et al., 2002) due to the highly complex solar magnetic field and transient phenomena sometimes disrupt the underlying structure. The Sun and the solar corona can be observed in various wavelengths and the interplanetary space can be studied by IPS (Inter-Planetary Scintillation) and by in-situ measurements. However, there are difficulties in identifying the correspondence between the source structure in the Sun-coronal region and the resultant structure in the interplanetary space because we can only infer the intrinsically three-dimensional structure of heliosphere from limited observations.

The heliospheric structure is largely determined by the solar magnetic field, and at the same time, it is true that the solar magnetic field is drawn outward by the supersonic solar wing plasma emanating through it. The formation of the heliospheric structure is the result of the integration of the topology of the solar magnetic field and the solar wind evolution there. Therefore, in order to obtain the full understanding of the heliospheric structure, it is necessary to consider the entire evolution of the solar wind describing accurately the coronal plasma process under the realistic solar magnetic field.

As for obtaining the heliospheric structure, there have been potential field models such as the PFSS (potential field source surface) model (Shatten et al., 1969; Altshuler et al., 1969), the PFCS (the potential field current sheet) model (Shatten et al., 1971), and Wang-Sheeley model (Wang and Sheeley, 1990). The PFSS model provides the coronal magnetic field by using the observed line-of-site (LOS) component of the photosphere magnetic field, under the assumption that the magnetic field is in potential field with purely radial at an outer spherical boundary, the so-called 'source surface.' In 1970, an idea that addresses a relationship between the coronal magnetic field and the solar wind speed was presented by Levine et al. (1977). They proposed that the solar wind speed is inversely correlated with the expansion rate of magnetic flux tube in the corona. This idea was quantitatively evaluated by Wang and Sheeley (1990), in which they derived the empirical relationship between the solar wind speed and the expansion rate of magnetic flux tube, the so-called 'expansion factor.' With subsequent updates (e.g., Zao and Hoeksema, (1995) for the PFSS model and e.g., Arge et al., (2000) for the Wang-Sheeley model), the PFSS and Wang-Sheeley models have been widely used as the practical way for the inferring the 3-D structure of the solar wind. However, it has been also discussed that the basis of the model itself, the coronal magnetic field described in the potential field, is debatable and that the model has an incompleteness in describing the plasma process important for the solar wind generation (the later point remains even in the case of the Current Sheet model (Shatten et al., 1971).

On the other hand, the mechanism of the solar wind acceleration has been one of the unsolved problems (the most difficult subjects) in solar physics and in physics of the solar wind. Most of the works associated with this topic have focused mainly on the high-speed component of the wind. As inferred originally by Parker's isotropic solution (Parker, 1958), the basis of the generation of the supersonic solar wind is the thermal driven mechanism. In this thermal driven mechanism, the high-

temperature coronal base is already assumed and the thermal conduction makes the coronal environment thermodynamically favorable for the supersonic evolution of the solar wind, maintaining the sufficient pressure gradient force against the solar gravity force. However, it is now generally recognized that additional source of momentum and/or energy is required at above the coronal base to account for the observed solar wind parameters at both the coronal base and the interplanetary space together with their radial profiles (Munro and Jackson 1977; Parker, 1991; Barnes et al., 1995). Many ideas have been suggested for the energy and direct momentum supply mechanisms. However, the entire scenario for the solar wind acceleration has still not obtained. The details and history of this subject are found in the review papers (e.g., Barnes, 1992; Hollweg and Isenberg, 2002; Cranmer, 2002).

The most effective way to organize magnetic field structure and plasma processes is the magnetohydrodynamics (MHD). Since from the pioneering work by Pneuman and Kopp (1971), a number of MHD models have been developed for the solar corona and the solar wind (e.g., Steinolfson et al., 1982; Washimi and Sakurai, 1993; Wang et al., 1998; Mikić et al., 1999; Linker et al., 1999; Usmanov, 1993a;1993b; Usmanov et al., 2000; Usmanov and Goldstein, 2003; Groth et al., 2000; Tóth et al., 2005; Feng et al., 2007). The development includes the sophistication from one-dimensional models to multi-dimensional models, from the simplified inner boundary condition to more realistic one, from the simplified treatment of the solar wind generation process to more detailed treatment, and from stationary problem to non-stationary one. Additionally, there are a wide variety of models, such as two-fluid (two-temperature) model (Suess et al., 1999), the chromospheric model including the coronal heating mechanism (Lionello et al., 2001), a semi-empirical model (Sittler and Guhathakurta, 1999) and so on.

Although the mechanism of the solar wind generation remains as the unsolved problem, MHD models can incorporate these unknown processes by parameterizations without explicitly specifying the physical mechanisms. Besides, by prescribing the inner boundary values with the observational data, MHD models can provide the realistic solution for the solar corona and solar wind.

As to the treatment of the solar wind generation, the most simplified way is to replace the ratio of specific heats (1+2/f, where f is the number of degrees of the freedom) with polytropic index in the energy equation. To mimic the thermodynamical process in which some external energy inputs exists, the polytropic index is set between 1 (corresponding to the isothermal process) to 1+2/f (equal to the ratio of specific heats, corresponding to the adiabatic process) (e. g., Usmanov, 1993a, b; Mikić et al., 1999; Linker et al., 1999; Riley et al., 2001). This simplified treatment of the energy equation succeeded in reproducing the general features of the solar corona and solar wind but suffered from failure to reproduce the quantitative properties of the solar corona and solar wind. Another way is to add parametric source functions in the energy and/or momentum equations. In the energy equation, an ad hoc volumetric heating function in the exponentially decaying form has been widely used (e.g., Wang et al., 1998; Sittler et al., 2002; Groth et al., 2000; Tóth et al., 2005; Feng et al., 2007). The modification of the momentum equation is also made by adding the momentum sources functions (Wang et al., 1998). Recently, in order to explicitly describe the solar wind acceleration process by Alfven waves, which is one of the promising candidates for efficient evolution of the supersonic flow (Belcher, 1971; Alazraki and Couturier, 1971), WKB approximation was incorporated in two-dimensional model by Usmanov et al. (2000) and in three-dimensional model by Usmanov and Goldstein (2003). These approaches using parametric functions or WKB approximation succeeded in obtaining quantitative features of the solar corona and solar wind, for example, the pair of high-speed wind and low-speed wind with their velocity and density contrast consistent with observations (e.g., Wang et al., 1998; Usmanov and Goldstein, 2003). However, in most cases, the solar magnetic field is simplified to the dipole field.

On the other hand, the use of the photospheric magnetic field data was initially made in 2-D model by Usmanov (1993a) and subsequently in 3-D model by Usmanov (1993b). Recent MHD models driven by the prescribed photosphere magnetic field are prominent in reproducing the realistic solar coronal structure (Mikić et al., 1999; Linker et al., 1999). However, in these models, the treatment of the solar

wind generation is usually simplified to the polytropic description. The detailed treatment of the solar wind generation and the use of observationally prescribed inner boundary do not go together because we have no conclusive answer relating these two.

Besides the above mentioned modeling subjects, in order to completely reproduce the entire structure of the Sun-solar wind system, it is also required to provide the sufficient simulation domain in 3-D. The simulation domains of models specific for the solar coronal region (Mikić et al., 1999; Linker et al., 1999; Wang et al., 1998; Feng et al., 2007) were up to about 30Rs at the furthest. Therefore, in terms of the validation with the in situ measurements in the interplanetary space, some ambiguities remain because some assumptions have to be made in drawing the model output to the spacecraft location and vice versa. On the other hand, 3-D and heliospheric simulation model have been presented by several workers. The large simulation domains have been achieved by splitting the simulation domain into inner part (sub-sonic and sub-Alfvenic region to super-sonic and super-Alfvenic region) and outer part (extend to several AU) (Usmanov 1993b; Riley et al., 2001; Usmanov and Goldstein., 2003) and recently by the adaptive-mesh refinement (AMR) technique (Gombosi et al., 2000; Groth et al., 2000; Tóth et al., 2005; Roussev et al., 2003; Cohen et al., 2007). In these heliospheric models, the simulation results were directly compared with in-situ observations, but the treatment of solar wind acceleration and the realistic solar magnetic field are still notcombined well. Gombosi et al., (2000), Groth et al., (2000), and Tóth et al., (2005) used the parametric functions for the solar wind generation, but their solar magnetic fields were simplified to multi-pole field. The photosphere magnetic field was used by gor example by Usmanov (1993b), Roussev et al. (2003), Cohen et al. (2007), and Riley et al. (2001). However, their solar wind generation is approximated to polytropic description although the polytropic index was varied with the distance from the center of the Sun. Also in the heliospheric model with WKB approximation by Usmanov and Goldstein (2003) the solar magnetic field is approximated to the dipole field, although the solar tilt is taken into consideration.

Summing up the above, it seems that the fully three-dimensional MHD model equipped with all of the use of the realistic solar magnetic field, the detailed treatment of solar wind generation process and the large simulation domain is not sufficiently prepared. With this point in mind, we have been developing a 3-D MHD simulation model for the Sun-solar wind combining system. In this paper we show the entire picture of the model and show a calculation result as the first result of the model. In Model Section we describe the details of the model. In Simulation Results Section we show simulation results for a specific time period (Carrington Rotation 2028) and evaluate the model by comparing the simulation results with the actual observations. In Discussion Section we give the discussion in the context of the future improvement of the model. Finally, Summary Section summarizes the contents of this paper.

2. Model

In this section we describe the details of the MHD simulation model. The unstructured computational grid that suits well with the Sun-solar wind system is firstly prepared (Section 2.1). The MHD solution is advanced in time by the modified MHD equations on the solar rotating frame (Section 2.2). The computational scheme performed on the unstructured grid system is a Finite Volume TVD scheme developed by Tanaka (1994) (Section 2.3). In order to obtain the realistic solution of the Sun-solar wind system we use the photosphere magnetic field data at the inner boundary (Section 2.4) and the introduce external source terms into the momentum and energy equation (Section 2.5)

2.1. Computational Grid

The computational grid for the Sun-solar wind model is required to reproduce the fine structure near

the Sun and the entire structure of the solar wind simultaneously. We developed such a computational grid based on the dodecahedron splitting method.

Figure 1 shows the generation process of the unstructured grid system starting from a regular dodecahedron (Fig. 1a). First, the pentagonal face of the dodecahedron is divided as shown in Fig. 1b. Five triangles are generated from one pentagonal face (first order splitting). The next step is to connect the midpoints of each side of the triangle. Four smaller triangles are generated from the former triangle as shown in Fig. 1c (second order splitting). At each step newly defined vertexes are projected on to the circumscribing sphere of the original dodecahedron, making the generated triangles the right triangles. This procedure can be repeated over and over until we obtain the sufficient fineness. Figure 1d-f show the thus generated triangle grid from 2nd, 3rd, and 4th order splitting, respectively. The sphere can be covered homogeneously by triangles of the same size without the directional dependence and without apparent singularity. Therefore, the computation is effectively stabilized.

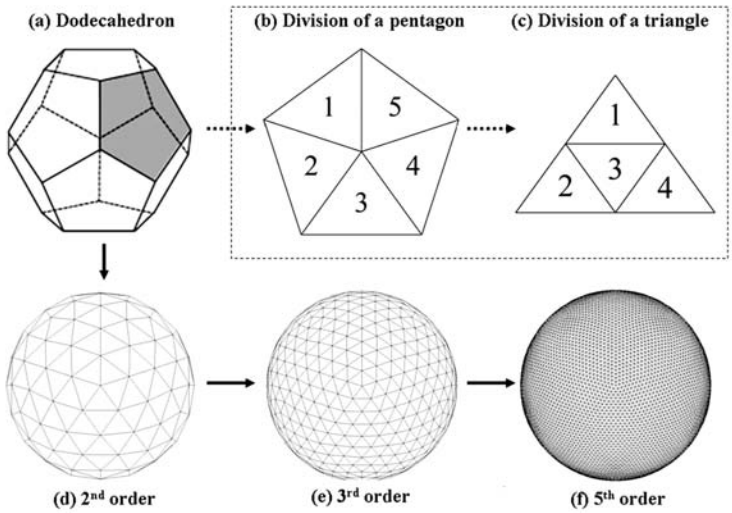

Fig. 1. The generation process of the unstructured grid system starting from a regular dodecahedron ((a)). (b) First, the pentagonal face of the dodecahedron is divided into five triangles (1st order splitting). (c) By connecting the midpoints of each side of the triangle, four smaller triangles are generated from the former triangle (2nd order splitting). In each step newly defined vertexes are projected on to the circumscribing sphere of the original dodecahedron, making the generated triangles the right triangles. This procedure can be repeated infinitely until we obtain the sufficient fineness. (d), (e) and (f) show the thus generated triangle grid from 2nd, 3rd, and 5th order splitting, respectively. The sphere can be covered homogeneously by triangles of the same size without the directional dependence and without apparent singularity.

Three dimensional grid system is obtained by stacking the above triangle mesh in the radial direction. This 3-D grid system is widely applicable to the 3-D system including the fine structure at its center, for example, the solar wind - planet interacting system. For the calculation of Sun-solar wind system, the Sun is placed at the innermost side of a numerical box, the outermost region is expanded according to our interest. This three-dimensional grid system can treat both of the fine structure near the Sun and the heliospheric structure expanding throughout the simulation domain simultaneously and, in addition, seamlessly. The calculation shown in this paper was performed on the 5th order splitting grid. In this splitting order, there are 7682 grid points and 15360 triangles on a sphere and the angular resolution is about 2.25 degree both in the latitudinal and longitudinal directions because the sphere is homogeneously filled by the triangle mesh. At present, we set the innermost to the coronal base and

outermost to the sphere with radius 200Rs. The spatial resolution in radial direction is gradually varied from 0.02Rs at the innermost to 1Rs at the outermost.

2.2. Equation System

The basic equations governing the Sun-solar wind system are the modified MHD equations written by dividing the magnetic field into a fixed potential magnetic field and the deviation component from it (Tanaka, 1994). These equations are:

$$\frac{\partial \rho}{\partial t} + \nabla \cdot (\rho \mathbf{v}) = 0, \tag{1}$$

$$\frac{\partial (\rho \mathbf{v})}{\partial t} + \nabla \cdot \left(\rho \mathbf{v}\mathbf{v} + P\mathbf{I} + \frac{B^2 - B_0^2}{2\mu_0}\mathbf{I} - \frac{\mathbf{B}\mathbf{B} - \mathbf{B}_0\mathbf{B}_0}{\mu_0} \right)$$

$$= -\rho \frac{GM_S}{R^2}\mathbf{r} - 2\rho \boldsymbol{\Omega} \times \mathbf{r} - \rho \boldsymbol{\Omega} \times (\boldsymbol{\Omega} \times \mathbf{r}) + S_M, \tag{2}$$

$$\frac{\partial \mathbf{B}_1}{\partial t} + \nabla \times (\mathbf{v} \times \mathbf{B}) = 0, \tag{3}$$

$$\frac{\partial U_1}{\partial t} + \nabla \cdot \left[\mathbf{v} \cdot \left(U_1 + P + \frac{B_1^2}{2\mu_0} \right) - \frac{\mathbf{B}_1 (\mathbf{v} \cdot \mathbf{B}_1)}{\mu_0} - \frac{\mathbf{B}_0 (\mathbf{v} \cdot \mathbf{B}_1)}{\mu_0} + \frac{\mathbf{v}(\mathbf{B}_1 \cdot \mathbf{B}_0)}{\mu_0} \right]$$

$$= \rho \mathbf{v} \cdot \left(-\frac{GM_S}{R^2}\mathbf{r} \right) - \rho \mathbf{v} \cdot [\boldsymbol{\Omega} \times (\boldsymbol{\Omega} \times \mathbf{r})] + S_E, \tag{4}$$

$$U_1 = \frac{P}{\gamma - 1} + \frac{\rho v^2}{2} + \frac{B_1^2}{2\mu_0} \tag{5}$$

where ρ, $\mathbf{V}$, and p are plasma mass density, bulk velocity and thermal pressure, respectively; $\mathbf{B}$, $\mathbf{B_0}$, and $\mathbf{B_1}$ are intensities of the total magnetic field, fixed potential magnetic field and deviation component from it ($\mathbf{B} = \mathbf{B_0} + \mathbf{B_1}$); U_1 is the modified total energy density, the summation of the kinetic energy density, thermal energy density and magnetic field energy density, written in terms of B_1. Other notations are the time t and the position vector from the solar center $\mathbf{r}$; μ_0 and R are the magnetic permeability in vacuum and the gas constant; G, Ms, and $\boldsymbol{\Omega}$ are the universal gravitational constant, solar mass and angular velocity of solar rotation; γ is the ratio of specific heats (equal to 1+2/f, where f is the number of degrees of freedom of plasma particle motion). The equations (1), (2), (3) and (4) correspond respectively to the continuity equation, momentum equation, induction equation, and energy equation of the basic MHD equations. They are written in the conservation form here. The terms S_M and S_E in the right hand side of the equation (2) and (4) are source terms for the solar wind acceleration. The details are described in Section 2.5.

The evolution of the solar wind is computed on a frame of reference co-rotating with the Sun, therefore, the rotational effects are included in the momentum and energy equations together with the effect of the solar gravity. The second and third terms in the right hand side of momentum equation are Coriolis and centrifugal forces. The second term in the right hand side of energy equation is the work done by centrifugal force. In the analysis of computational results, the calculated data is transformed to the coordinate system at rest so that these apparent rotational effects are removed.

Originally MHD equations are derived by taking the velocity moment of the Boltzmann equation. Thus derived macroscopic equations are not a closed set, because i-th order equation contains the next order (i+1) variables. To close the equation system the derivation is truncated at a certain order with

some approximation for dealing the higher order variables (e.g., Schunk, 1977). The most simplified way is to replace the energy equation (second order moment equation) with the equation of state

$$P = \alpha \rho^{n}, \tag{6}$$

where α is a constant of fluid elements. In this formulation the description of the thermodynamical property of MHD fluid is entrusted to n (The equation represents the thermodynamical processes by giving the relationship between the plasma density and pressure variations through the index n.). In this sense n is called as polytropic index (Siscoe, 1983). In the adiabatic assumption n becomes purely equal to the ratio of specific heats. This adiabatic truncation is equal to the use of the set of ideal MHD equations (conservation equations with no source terms). In other words, by replacing the ratio of specific heats γ in MHD equation system with the polytropic index n we describe thermodynamical processes approximately, without specifically introducing external source terms. In this paper we introduce external source terms (S_M and S_H) rather than adjusting γ. Therefore γ in the above equation system remains to be the ratio of specific heats. We set γ to 5/3 assuming the monatomic and isotropic plasma.

2.3 Computational Scheme

The time integration of the above MHD equation system is performed by a Finite Volume Method (FVM) originally developed by Tanaka (1994). Numerical fluxes for FVM are written in upwinding form based on the eigenmode decomposition (Brio and Wu, 1988) and calculated by Total Variation Diminishing (TVD) scheme with Monotonic Upstream Scheme for Conservation Laws (MUSCL) interpolation with Van-Leer's differentiating limiter. For details of the entire of the scheme, see Tanaka (1994).

The control volume essential for the FVM is illustrated in Fig. 2. Solid lines are gird on a sphere, and dotted lines are their projection on interfacing surfaces between spheres. By connecting the circumcenters of triangles neighboring the grid point, the control volume is defined (the hexagonal column shown by thick lines). Variations of physical quantities at the grid point are computed by summation of numerical fluxes over all faces of the control volume.

2.4. Boundary Condition and Initial Condition

To begin the MHD computation, we require the boundary condition and initial condition. The set of boundary condition used in the present study is summarized in Table 1. $V_{\parallel}$ is the field aligned component of **V**. $V_{\perp 1}$ and $V_{\perp 2}$ are the field perpendicular components of **V**. $B_{1,\,r}$ is the radial component of $\mathbf{B_1}$. $B_{1,\,t1}$ and $B_{1,\,t2}$, are residual components of $\mathbf{B_1}$ tangential to the spherical surface. $B_{0,\,LOS}$ is the Line-Of-Site component of $\mathbf{B_0}$ and $B_{0,\,1}$ and $B_{0,\,2}$ are its residuals (The reason for this $\mathbf{B_0}$ decomposition will be found below.). At the outer boundary, the variable on which the Dirichlet condition is imposed is U_1, being determined so as the plasma pressure asymptotically approaches to 0 (Parker, 1958). All other variables are solved under the Neumann condition. At the inner boundary, $V_{\parallel}$, $B_{1,\,t1}$, and $B_{1,\,t2}$ are also solved under the Neumann condition, while ρ, $V_{\perp 1}$, $V_{\perp 2}$, $B_{1,\,r}$, and U_1 are subject to the Dirichlet condition. In order to reproduce the Sun-solar wind structure realistically, we specified the inner boundary magnetic field with the photospheric magnetic field data. In this study we used the LOS photosphere magnetic field data provided by Wilcox Solar Observatory (2008) (http://wso.stanford.edu/) for the specification of $B_{0,\,LOS}$. $B_{1,\,r}$, $V_{\perp 1}$ and $V_{\perp 2}$ are fixed to 0 so as not to permit the addition of magnetic fluxes that are unphysical and inconsistent with the prescribed $B_{0,\,LOS}$. ρ is fixed to 1.5×10^{-13} kg m^{-3} (number density of 0.9×10^{14} m^{-3}) and U_1 is automatically determined by other variables with reference temperature T_0=0.5×10^{6} K.

The MHD computation is initiated with the following conditions: ρ and p are in hydrostatic equilibrium, **B** is set to potential field, and **V** is set to zero. The potential magnetic field consistent with

Table 1. Boundary conditions for MHD equation system.

	Inner Boundary 1 Rs	Outer Boundary 200 Rs
ρ (mass density)	fix	$\partial/\partial r=0$
$V_{\parallel}$ (parallel to **B**)	$\partial/\partial r=0$	$\partial/\partial r=0$
$V_{\perp,1}$ (perpendicular to **B**)	0	$\partial/\partial r=0$
$V_{\perp,2}$ (perpendicular to **B**)	0	$\partial/\partial r=0$
$B_{1,r}$ (radial component)	0	$\partial/\partial r=0$
$B_{1,t1}$ (residual of $\mathbf{B}_1$)	$\partial/\partial r=0$	$\partial/\partial r=0$
$B_{1,t2}$ (residual of $\mathbf{B}_1$)	$\partial/\partial r=0$	$\partial/\partial r=0$
U_1 (modified total energy density)	fix	fix ($p\rightarrow 0$)
$B_{0,LOS}$ (Line-Of-Site component)	fix (observation)	Free
$B_{0,1}$ (residual of $\mathbf{B}_0$)	Free	Free
$B_{0,2}$ (residual of $\mathbf{B}_0$)	free	Free

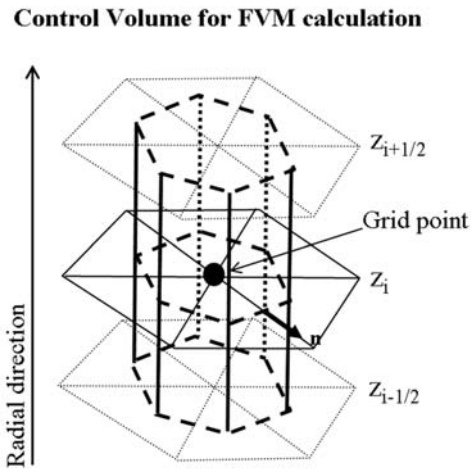

Fig. 2. The control volume essential for the FVM calculation. Black solid lines are gird on a sphere, black dotted lines are their projection on interfacing surfaces between spheres. By connecting the circumcenters of triangles neighboring the grid point, a hexagonal column is defined as depicted by thick lines. This hexagonal column is the control volume. Variations of physical quantities at the grid point are computed by summation of numerical fluxes over all faces of the control volume.

the boundary values specified by the observational data are obtained by conjugate residual (CR) method. Under the aforementioned boundary and initial conditions, the MHD equation system is advanced in time until the steady-state is reached. We regard the obtained steady-state solution as a basic structure of the heliosphere during the period of observational data $B_{0,LOS}$ used for the inner boundary. Therefore, time-dependent problems, such as the eruption and propagation of CMEs, are beyond the scope of this paper.

2.5. Approach for Solar Wind Acceleration under the Realistic Solar Magnetic Field

In order to obtain the realistic acceleration of the solar wind, we have incorporated external source terms into the momentum and energy equation. The energy source term consists of the set of ad hoc volumetric heating function (the first term) and thermal conduction term of Spitzer type (the second term),

$$S_E = Q_o (R - 1.0) \exp(-R/L_Q) + \nabla\left(\xi T^{2.5} \frac{\nabla T \cdot \mathbf{B}}{B^2}\right) \cdot \mathbf{B}, \quad (7)$$

where R is the distance from the center of the Sun normalized by solar radius, Q_0 and L_Q are the intensity and decay length of heating, and T is temperature. The heat conduction of collision-less regimes is not included in the present model. Although this exponential decaying form of the heating function originated with Hartle and Barnes (1970) and has been widely used (e.g., Suess et al., 1996; Wang et al, 1998; Groth et al., 2000), we take the topology of magnetic field into consideration, which is a new idea. We inversely proportionate the heating intensity Q_0 with the expansion factor *fs* defined below,

$$f_S = \left(\frac{Rs}{R}\right)^2 \frac{B_{Rs}}{B_R}. \quad (8)$$

Where *Rs* and *R* are the solar radius and the distance from the solar center, and B_{Rs} and B_R are magnetic field strength at the solar surface and at *R.* The idea is motivated by the inverse relationship between the solar wind speed and the expansion factor (Levine et al., 1977; Wang and Sheeley, 1990). From this adjustment, the heating is diminished at the location where the magnetic field is in over-radial expansion (*fs* > 1.0), and also it is intensified at the location where the magnetic field in under-radial expansion (*fs* < 1.0), leading to the heating distribution that is not uniform or simply dependent only on the latitude but reflecting the topology of magnetic field in the key region of the solar wind generation.

The momentum source term is written in the similar form as that of the heating function

$$S_M = M_o (R - 1.0) \exp(-R/L_M). \quad (9)$$

Where M_0 and L_M are the intensity and the decay length of the momentum addition. M_0 is also adjusted by the expansion factor *fs* in the same way as in the heating term. In the present calculation, Q_0 and M_0 are set to 3.3×10^{-6} $Jm^{-3}s^{-1}$ and 5.3×10^{-14} Nm^{-3}, and L_Q and L_M are set to 0.9 Rs.

3. Simulation Results

In this section we show the simulation results for the data period of Carrington Rotation 2028 (from March 24 to April 21, 2005). First we focus on the fine structure of the solar corona then we move to the heliospheric structure of the solar wind. The capability of the 3D MHD model is evaluated by making comparisons with actual observations.

3.1. Fine structure of the solar corona

Figure 3 (a) shows a close up view of the Sun-inner corona visible from the Earth on 3 April, 2005 (corresponding to Carrington longitude of about 240 ^{o}). The color shading shows the intensity of radial plasma flux on the sphere with radius 1.5 Rs. High outward flux areas are shown by red and yellow change to semi-color; low flux areas are shown by blue and green. The color code is given at the bottom of the figure. Blue and red lines are magnetic field lines traced up from the solar surface. Blue lines are "toward" field lines and red lines are "away" field lines. The contour surface indicates the isothermal surface of $T = 2.0 \times 10^6$ K and the interior of the surface is high-temperature regions ($T > 2.0 \times 10^6$ K).

We can observe that each group of open field lines of the same polarity originates each continuous area on the sphere separated by contour surfaces. In other words, the contour surface represent the boundary between closed and open field lines and its insides correspond to the closed field regions where the coronal plasmas are heated due to the confinement by magnetic tension force. Also we can see that open field lines can be traced back to warm color areas where solar plasma is exiting to outer space. It indicates that the solar wind plasma and interplanetary magnetic field are supplied from warm

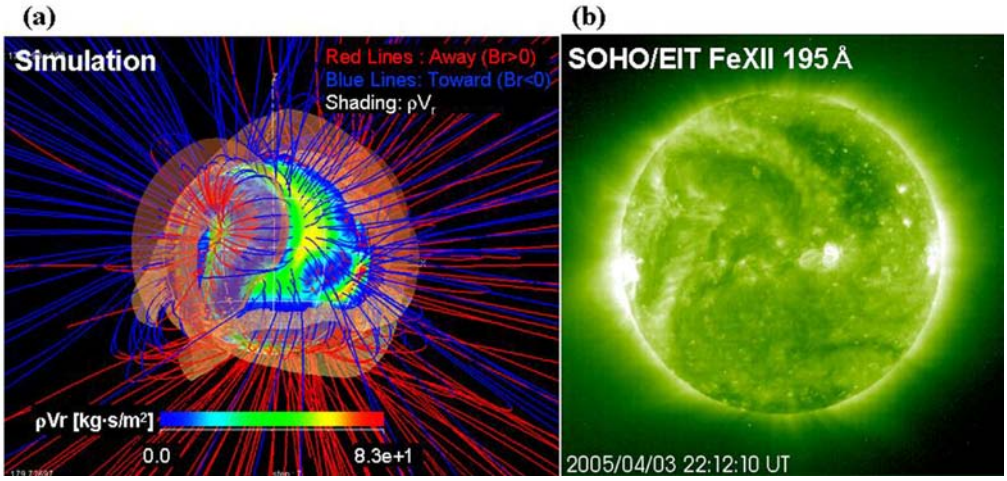

Fig. 3. (a) A close up view of the simulated sun-inner corona visible from the Earth on 3 April, 2005 (corresponding to Carrington longitude of about 240 degree). The color shading shows the intensity of radial plasma flux on the sphere with radius 1.1 Rs. High outward flux areas are shown by red and yellow, and low flux areas are shown by blue and green. The color code is given at the bottom of the figure. Blue and red lines are tracing of magnetic field lines traced up from anchored at the solar surface. Blue lines are "toward" field lines and red lines are "away" field lines. The contour surface indicates the isothermal surface of $T = 2.0 \times 10^6$ K and the interior of the surface is high-temperature regions ($T > 2.0 \times 10^6$ K). Alternating pattern between open and away field lines separated by contour surface is observed. Each group of open field lines of the same polarity originates each continuous compartment on the sphere separated by the foot of contour surface. Also we can see that open field lines can be traced back to warm color areas where solar plasma is exiting to the outer space. It indicates that the solar wind plasma and interplanetary magnetic field are supplied from warm color areas. These high mass flux areas are considered to be representing coronal holes from which the solar magnetic field is opened and stretched out toward the interplanetary space by the exiting solar wind plasma. (b) An image provided by the EIT instrument on board SOHO on April 3, 2005 (corresponding to Carrington longitude ~240 degree) for the reference of (a). Coronal holes are recognized as dark low-emission regions and active regions are recognized by bright intense-emission regions. A prominent coronal hole can be seen in the northern hemisphere. Turning back to (a), we can also notice a large outward flux area formed in the northern hemisphere. By comparing (a) and this image, it is concluded that the calculated coronal hole closely resembles to the coronal hole identified by SOHO/EIT observation, both in the shape and location.

color areas. Therefore. these areas are considered to be representing coronal holes from which the solar magnetic field is opened and stretched out toward the interplanetary space by exiting solar wind plasma.

For the reference of the calculated Sun-solar corona, Fig. 3b presents an image provided by the EIT instrument on board SOHO on April 16, 2005 (corresponding to Carrington longitude ϕ ~120 ^{o}). In EIT images, coronal holes are recognized as dark low-emission regions and active regions are recognized by bright intense-emission regions. In Fig. 3b a prominent coronal hole can be seen in the northern hemisphere. Turning back to the Fig. 3a, we can also notice a large outward flux area formed in the northern hemisphere. By comparing Fig. 3a and Fig. 3b, it is concluded that the calculated coronal hole closely resembles to the coronal hole identified by SOHO/EIT observation, both in the shape and location. We checked all sides of the calculated Sun in the same way and confirmed that coronal holes obtained by the simulation are in good agreement with those observed by the SOHO/EIT.

We can observe from Fig. 3a that all of the characteristic structures, such as high-temperature region associated with closed loops, plasma exiting areas and the alternating pattern between open and away field lines separated by contour surface, are organized in the Sun-solar corona combining system. This organized structure consequently spread over the interplanetary space, defining the heliospheric structure as shown in the next section. The current model does not describe the physics under the coronal base including transition region chromosphere, and photosphere. Therefore, the short-loop structure related to

active regions and its dynamical properties can not be treated in the present simulation.

3.2. 3-D structure of the solar wind

Figure 4 shows the solar wind structure in the equatorial plane. Now the Sun is located at the center of the plane and the outer circumference corresponds to the circle of radius 200Rs, which is close to the terrestrial orbit. White lines indicate the Carrington longitudes 360, 270, 180, and 90 degree. These longitudes faced the earth on March 25, April 1, April 8, and April 15, respectively. The contour line shows the radial component of the solar wind velocity: high-speed regions with red and yellow, and low-speed regions with blue and green. The color code is shown at the bottom of the figure. The sector polarity is also shown by color shading: "away" polarity with red and "toward" polarity with blue, the same as in Fig. 3a. We can see from this figure that the interplanetary space during this period is characterized by three large sectors accompanied by high-speed solar wind and a small-scale sector without high-speed solar wind.

Next, we evaluate the simulation result quantitatively. The simulation data on the outer circumference of the computational domain is subject to the comparison with the in-situ measurement at L1 point. Figure 5 shows the comparison between simulation data and the observational data obtained by the ACE satellite. Horizontal axis is the time from March 29 to April 24, 2003. Before proceeding to the comparison, we write up the general feature of the solar wind observation during this period. Figure 5a shows the 1-hour averaged data of the ACE satellite: shown from the top to bottom column are, the radial component of solar wind speed, Vr, the proton density, Np, and the angle between the magnetic field and the GSM-X axis,ϕ, indicating the sector polarity. The solar wind during this period is characterized by three sets of the high-speed wind forming the well-defined large scale sectors with CIRs (co-rotating interaction region) being evolved in front of it. The field polarity of first, second and third high-speed regions are away toward, and toward. The boundary between the first and second sector is clear with no contamination of small scale structure. On the other hand, the boundary between the second and third high-speed wind seems to be interrupted by the small reversed (away) polarity field. This small scale structure is considered to be a slight encounter of the heliospheric neutral sheet because the proton density is high and the solar wind speed remains to be slow.

The direct comparison between the simulation results and observational data are given in Fig. 5b. The figure format is the same as in Fig. 5a. The simulation data and observational data are superimposed upon in each of the columns: the black dots are 1-hour averaged ACE data as the same as in Fig. 5a, the thin solid lines are 1-day averaged ACE data, and thick solid lines are the simulation data. The calculated solar wind data match well with the observational data. The first, second, and third high-speed wind seen in the observation are successfully reproduced in the simulation together with their sector polarity. The small away sector between second and third toward sector is also reproduced. We can see better agreement between simulation data and 1-day averaged data. This is related to the spatial and time resolution of the present simulation. The circumferential resolution of the computational space is equal to the time resolution of the virtual solar wind observed by the ACE satellite because we regard the MHD solution as the quasi-steady structure of the interplanetary space during the period of interest. Thus, the angular resolution of about 2.25 degree (that we mentioned in section 2.4.) is equal to about 4.05 hours in terms of the time resolution, being translated with the solar rotation period relative to the earth. Therefore, solar wind structures observed in a few hours are considered to be smoothed out in the present simulation. For example, CIR associated features, such as density enhancement in front of the high-speed wind and the leading edge of the high-speed wind, are clearly observed in 1-hour averaged data but their sharpness are lost in the simulation data. The rate of the density enhancement and the slope of the rise of the solar wind speed of the simulation data are close to those of the 1-day averaged data rather than those of the 1-hour averaged data.

Irrespective of the smoothing effect by the limitation of the spatial and time resolution, there exist

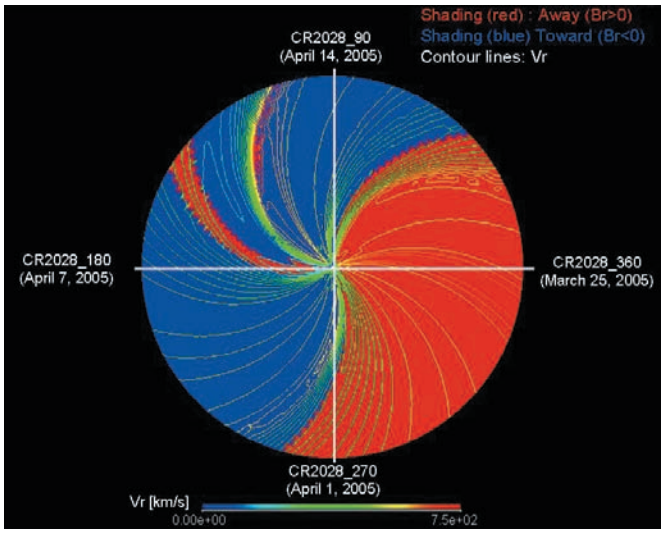

Fig. 4. The entire structure of the simulated solar wind in the equatorial plane. The Sun is located at the center of the plane and the outer circumference corresponds to the circle of radius 200Rs, which is close to the terrestrial orbit. White lines indicate the Carrington longitudes 360, 270, 180, and 90 degree. These longitudes faced the earth on March 25, April 1, April 7, and April 14, respectively. The contour line shows the radial component of the solar wind velocity: high-speed regions with red and yellow and low-speed regions with blue and green. The color code is shown at the bottom of the figure. The sector polarity is also shown by red and blue color shading: "away" polarity with red and "toward" polarity with blue, as the same as in figure 3(a). We can see from this figure that the interplanetary space during this period is characterized by large three sectors accompanied by high-speed solar wind and a small-scale sector without high-speed solar wind.

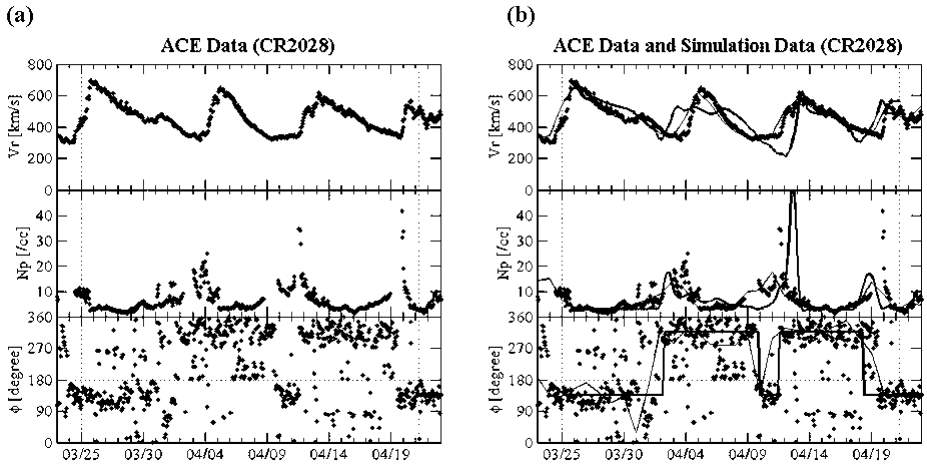

Fig. 5. (a) The 1-hour averaged data of the ACE satellite during March 23 to April 23, 2005. Shown from the top to bottom column are, the radial component of solar wind speed, Vr, the proton density, Np, and the angle between the magnetic field and the GSM-X axis, ϕ, indicating the sector polarity. The vertical dashed lines indicate the start and end time of the CR2028 (start time is 01:00 on March 25, 2005 and end time is 07:00 on April 21, 2005). The solar wind during this period is characterized by three sets of the high-speed wind forming the well-defined large scale sectors with CIRs (co-rotating interaction region) being evolved in front of it. The field polarity of first, second and third high-speed regions are away toward, and toward. The boundary between the first and second sector is clear with no contamination of small scale structure. On the other hand, the boundary between the second and third high-speed wind seems to be interrupted by the small reversed (away) polarity field. This small scale structure is considered to be a slight encounter of the heliospheric neutral sheet because the proton density is high and the solar wind speed remains to be slow. (b) The direct comparison between the simulation data and observational data. The Figure format is the same as in (a). The simulation data and observational data are superimposed upon in each of the columns: the black dots are 1-hour averaged ACE data as the same as in (a), the thin sold lines are 1-day averaged ACE data, and thick solid lines are the simulation data.

some discrepancies between the simulation and the observation. One of them is the timing of the arrival of the fast wind. In the simulation, the second fast wind is shifted forward by about 2-3 days. The other discrepancy is the concern about the absolute value of the solar wind speed. The speed of the simulated second fast wind is about 120 km/s lower than that of the observation and the slow wind between the second and third fast wind is estimated much lower than the actual wind. These discrepancies are considered to be related to the solar wind acceleration process and interaction process between fast and slow winds. We will improve the model by the parameterization, the refinement of the computational grid in the future work. However, it should be mentioned that the present MHD model can avoid resulting in unrealistic high-density values and lack of speed contrast between fast and slow wind that have been often reported in polytropic models (e.g., Usmanov, 1993).

4. Discussion

In the previous section, it is confirmed from the data comparison that the MHD model successfully reproduced many features for both of the solar coronal region and the solar wind 3-D structure. However, the model needs further improvement before being applied directly to the study of the Sun-earth connection.

4.1. Inner boundary condition and MHD sensitivity for plasma beta

When we start an MHD simulation of the Sun-solar wind system, we require boundary values for plasma parameters and magnetic field at the inner boundary. In this study, the magnetic field at the inner boundary has been specified by observed photospheric magnetic field. On the other hand, plasma parameters such as proton density and temperature have been only assigned by uniform quantities, as has been done in previous works ($\rho=1.5 \times 10^{-13}$ kg m^{-3} and $To=0.5 \times 10^{6}$ K, in the present paper). Although this is an over simplification, the MHD model could reproduce the overall picture of solar corona and solar wind. It seems more important to choose the density and temperature values so that the plasma beta (the ratio of plasma thermal pressure and magnetic pressure) becomes a proper value for the coronal region rather than specifying the fine distribution. That is because the MHD solution is very sensitive to the plasma beta and plasma beta determines the effectiveness of parameterized source functions.

First, we consider the sensitivity of the MHD solution to the plasma beta. Linker et al. (1999) tested this aspect by using the PFSS model outputs as a proxy for how the MHD solutions are affected by plasma beta. In PFSS model the height of source-surface (Rss) influences the position and shape of coronal holes. As the values of Rss decrease (increase) coronal holes become larger (smaller). Similarly in MHD model, it is expected that the increase (decrease) in the plasma density and temperature at the inner boundary, coronal base, results in yielding the larger (smaller) coronal holes (Linker et al., 1999). Lowering the Rss is equivalent to emphasizing the plasma forces because the solar magnetic field is forcibly opened at relatively low altitude and small scale structures associated with local strong magnetic field are stuck beneath the source surface. Raising the Rss is equivalent to reducing the plasma forces, vice versa. In this way, the plasma beta in MHD simulations and Rss (altitude of source surface) in PFSS models have similar influence on the model solution. Considering that the PFSS model outputs are altered by the altitude of Rss, we have to set the plasma beta carefully. When the plasma beta is chosen properly it is likely to be one of the pragmatic ways to adopt the observation-based boundary conditions suggested by Hayashi et al. (2005).

Although the discussion for the solar wind acceleration is given in the next section, here we briefly mention that Rss in PFSS model also include the similar effect of the external source terms in MHD simulation. In the first place, it seems to be natural to set Rss to Alfven point (5-10 Rs) because the

boundary condition imposed at Rss means that the magnetic force have no importance in determining the structure outward of Rss. However, Rss is set to much lower altitude (usually to 2.5 Rs) and the model reproduce the heliospheric structure rather well. This fact indicates that PFSS models can estimate the coronal plasma forces quite accurately through the setting of Rss although they do not describe the plasma process explicitly. We should develop MHD models bearing in mind that they should reproduce better results than PFSS models when the plasma beta and external source terms are chosen properly.

In addition to the simplification of the uniform density and temperature distribution, the present model places its inner boundary not on the solar surface (1.0 Rs) strictly but on the so-called coronal base (~1.01Rs) as is usual in 3-D MHD models. It means that the 3-D MHD simulation generally stands on the already heated corona and smoothed inner boundary neglecting microscopic structures underneath the coronal base (The reference temperature value 0.5×10^6 K adopted in the present simulation is much lower than that of previous 3-D models. Therefore we could say that the present model could approach to some extent to the solar wind acceleration from just beneath the coronal base). The precise description for transition region, chromosphere, and photosphere is needed to understand coupling processes among these regions, coronal heating mechanism and the resultant coronal dynamics. The chromospheric model by Lionello et al. (2001) is the first attempt in this direction in the multi-dimensional model.

4.2. Parameterization for solar wind acceleration

One of the most important problems in the Sun-solar wind modeling is the treatment of the solar wind acceleration. In 3-D MHD simulations, the use of photospheric magnetic field data and the use of the parametric source terms for solar wind acceleration do not coexist because there is no definitive answer for how we should do the parameterization in conformity with an actual magnetic field configuration. In this study, we incorporated the parametric source functions into the momentum and energy equations. Although they are in the widely-used form, we have newly adjusted their intensities by using the expansion factor *fs*. Our idea is based on the inverse-relationship between *fs* and the solar wind speed that have been widely accepted since Levine et al.'s work (Levine et al., 1977). Our expectation is that we have flow speed variations according to the topology of the realistic solar magnetic field and the result shows that this method works well. However, we should carefully apply *fs* to parameterizations considering the following. We consider the case where the source term is only the volumetric heating term. Inside the flux tube of small *fs*, the heating addition is intensified then the pressure gradient force is maintained relatively to a higher altitude by the thermal conduction along the magnetic field. Inside the flux tube of large *fs*, the pressure gradient force would decreases faster, and vice versa. This tendency seems to be convenient for having the variation of solar wind speed that is consistent with the inverse relationship between *fs* and the solar wind speed. However, it should be remembered that the behavior of the solar wind plasma is affected by whether the external energy is deposited in the subsonic region or supersonic region. Generally, the heating addition raises the density scale height. This means that the heating addition in the subsonic region lowers the asymptotic solar wind speed (compared with the plasma without heating addition) because the kinetic energy per particle is decreased in the denser plasma. Only the excessive intensification of the heating by *fs* can yield the result opposite to our expectation. It is necessary for the efficient solar wind acceleration not to raise the plasma density so much in the subsonic region.

The direct momentum addition that we have done in this study is one way to avoid the aforementioned inconvenience and the result was quite good. However, our parameterization is not definitive yet as was shown by the data comparison in Section 3.2. The most straightforward way of improving the parametric function would be to accurately incorporate results of theoretical works. For example, Withbroe (1988) derived energy input profile that is required to account for the efficient acceleration. However, most of these theoretical works have been intended for the large polar coronal

hole seen during the solar minimum. What we must do now is to predict the solar wind under the various solar activity phases. It is necessary to establish the universal parameterization that works well in every topology of solar magnetic field. A recent study with 1-D MHD simulation succeeded in reproducing the solar wind acceleration process by self-consistently describing low frequency MHD waves (Suzuki et al., 2005). The future direction of the sophistication of 3-D models will be the association with these 1-D models that can treat the middle-scale processes from which the parameterization in 3-D models should be determined.

4.3. Application to integrated numerical simulation system of the Sun-solar wind-earth system

Starting from the pioneering work by Usmanov (1993a, 1993b), heliospheric MHD models that are designed to simulate the solar surface to the earth's orbit and beyond have been developed. These include the solar corona-inner heliosphere coupled model (e.g., Odstrcil et al., 2004) and unified model based on the AMR (adaptive mesh refinement) technique (Groth et al., 2000; Tóth et al., 2005). With the recent promotion of the space-weather research, CME erupting events have been simulated by these models (e.g., Tóth et al., 2005). In these studies, the underlying solar wind structure is usually reduced to that of solar minimum. Actually, the occurrence of CME eruptions is more frequent in solar maximum and declining phases rather than solar minimum phase. As was pointed out by Usmanov and Dryer (1995), the sophistication of the modeling of the solar wind structure consistent with the actual solar magnetic field have equal importance with the CME simulation because the precise understanding of the CME propagation and deformation can not be obtained without their interaction with the underlying structure of the solar wind. We are firstly directed to this goal. In the near future the model will be applied in the integrated space weather simulation system being developed at NiCT (National institute of Information and Communication Technology), Japan.

Presently, the computation is performed on the 5th-order splitting grid. In this splitting order, the angular resolution is about 2.25 degree and this is equal to about 4.05 hours in terms of the time resolution, as we already noted in Section 3.2. This time scale is much longer than that of various geomagnetic phenomena. For example, geomagnetic storms occur on a time scale of about a few hours to a day but it is the variation of solar wind in the time scale of a few tens of minutes that control their growth and decay. Therefore, even the solar wind and IMF variations related to the largest event in the Sun-earth system cannot be sufficiently reproduced under the present grid resolution. Furthermore, magnetospheric substorms, of whose time scale is about a tens of minutes to a few hours, is critically controlled by the solar wind in the time scale of a few tens of minutes. We are now preparing to proceed to the higher-order splitting grid.

5. Summary

We have been developing a 3-D MHD model of the Sun-solar wind combining system. In this paper, we have described the overall picture of the MHD model and we have given the result for a specific time period (CR2028). The characteristics of the model are summarized as follows:

(1) The computational grid is an unstructured grid system based on the dodecahedron splitting method. The advantages of this grid system are twofold: (a) The computation is effectively stabilized with no apparent singularity; and (b) The fine structure near the Sun and the heliospheric structure can be handled together on the grid mesh seamlessly constructed from the inner boundary to outer boundary.

(2) The magnetic field at the inner boundary is prescribed with the observational data of photospheric magnetic field during a specific time period.

(3) For the generation of the supersonic solar wind the parametric external source terms are introduced into the energy equation and momentum equation. The source functions have the form of exponentially

dumping as has been widely used in the previous works.
(4) The intensities of the source functions are adjusted so as to reflect the topology of the coronal magnetic field. They are increased inside the magnetic flux tube in sub-radial expansion and reduced inside the magnetic flux tube in over-radial expansion.

It is confirmed from the data comparison that the MHD model successfully reproduced many features both of the solar coronal region and the heliospheric structure. In the solar coronal regions, the large-outward mass flux areas on the simulated solar surface closely resemble coronal holes recognized by SOHO/EIT image, in both of the shape and location. The simulated variations of solar wind parameters and the magnetic field polarity are in good agreement with the ACE observations, although there are still some discrepancies.

In conclusion, it has been confirmed that the model has the capability to treat the solar wind generation process and the 3-D structure consistent with the solar magnetic field in a unified manner. With the further improvement and refinement, the model will be applied to the integrated space weather simulation system being developed in NiCT, in Japan.

6. Acknowledgements

Wilcox Solar Observatory data used in this study were obtained via the web site http://quake.stanford.edu/~wso courtesy of J.T. Hoeksema. We also thank the ACE/SWEPAM and MAG instrument teams and the ACE Science Center for providing the ACE data. We wishes to thank the anonymous referee for his/her careful reading of the manuscript and making a number of useful comments employed in the subsequent revisions.

7. References

Alazraki, G., and Couturie, P. (1971) Solar wind acceleration caused by gradient of Alfven wave pressure, *Astron. Astrophys., 13*, 380.

Altschuler, M. D., and Newkirk, G.(1969) Magnetic fields and structure of solar corona .I. methods of calculating coronal fields, *Sol. Phys., 9*, 131.

Arge, C. N., and Pizzo, V. J. (2000) Improvement in the prediction of solar wind conditions using near-real time solar magnetic field updates, *J. Geophys. Res., 105* (A5), 10465.

Barnes, A. (1992) Acceleration of the solar-wind, *Rev. Geophys., 30* (1), 43.

Barnes, A., Gazis, P. R., and Phillips, J. L. (1995) Constraints on solar-wind acceleration mechanisms from Ulysses plasma observations - the first polar pass, *Geophys. Res. Lett., 22* (23), 3309.

Belcher, J. W. (1971) Alfvenic wave pressures and solar wind, *Astrophys. J., 168*, 509.

Brio, M., and Wu, C. C. (1988) An upwind differencing scheme for the equations of ideal magnetohydrodynamics, *J. Comput. Phys., 75*, 400.

Cohen, O., Sokolov, I. V., Roussev, I. I., Arge, C. N., Manchester, W. B., Gombosi, T. I., Frazin, R. A., Park, H., Butala, M. D., Kamalabadi, F., and Velli, M. (2007) A semiempirical magnetohydrodynamical model of the solar wind, *Astrophys. J., 654*, L163.

Cranmer, S. R. (2002) Coronal holes and the high-speed solar wind, *Space Sci. Rev., 101*, 229.

Feng, X. S., Zhou, Y. F., and Wu, S. T. (2007) A novel numerical implementation for solar wind modeling by the modified conservation element/solution element method, *Astrophys. J., 655*, 1110.

Gombosi, T. I., DeZeeuw, D. L., Groth, C. P. T., Powell, K. G., and Stout, Q. F. (2000) Multiscale MHD simulation of a coronal mass ejection and its interaction with the magnetosphere-ionosphere system, *J. Atmos. Sol.-Terr. Phys., 62*, 1515.

Groth, C. P. T., DeZeeuw, D. L., Gombosi, T. I., and Powell, K. G. (2000) Global three-dimensional MHD simulation of a space weather event: CME formation, interplanetary propagation, and interaction with the magnetosphere, *J. Geophys. Res., 105* (A11), 25053.

Hartle, R. E. and Barnes, A. (1970) Nonthermal heating in 2-fluid solar wind model, *J. Geophys. Res., 75* (34), 6915.

Hayashi, K. (2005) Magnetohydrodynamic simulations of the solar corona and solar wind using a boundary treatment to limit solar wind mass flux, *Astrophys. J. Suppl. Ser., 161*, 480.

Hollweg, J. V. and Isenberg, P. A. (2002) Generation of the fast solar wind: A review with emphasis on the resonant cyclotron interaction, *J. Geophys. Res., 107* (A7), 1147, doi:10.1029/2001JA000270.

Levine, R. H., Altschuler, M. D. and Harvey, J. W. (1977) Solar sources of interplanetary magnetic-field and solar-wind, *J. Geophys. Res., 82* (7), 1061.

Linker, J. A., Mikić, Z., Biesecker, D. A., Forsyth, R. J., Gibson, S. E., Lazarus, A. J., Lecinski, A., Riley, O., Szabo, A., and Thompson, B. J. (1999) Magnetohydrodynamic modeling of the solar corona during Whole Sun Month, *J. Geophys. Res., 104* (5), 9809.

Lionello, R., Linker, J. A., and Mikić, Z. (2001) Including the transition region in models of the large-scale solar corona, *Astrophys. J., 546*, 542.

McComas, D. J., Bame, S. J., Barraclough, B. L., Feldman, W. C., Funsten, H. O., Gosling, J. T., Riley, P., Skoug, R., Balogh, A., Forsyth, R., Goldstein, B. E., and Neugebauer, M. (1998) Ulysses'return to the slow solar wind, *Geophys. Res. Lett., 25* (1), 1.

McComas, D. J., Elliott, H. A., Gosling, J. T., Reisenfeld, D. B., Skoug, R. M., Goldstein, B. E., Neugebauer, M., and Balogh, A. (2002) Ulysses' second fast-latitude scan: Complexity near solar maximum and the reformation of polar coronal holes, *Geophys. Res. Lett., 29* (9), 1290, doi:10.1029/2001GL014164.

Mikić, Z., Linker, J. A., Schnack, D. D., Lionello, R., and Tarditi, A. (1999) Magnetohydrodynamic modeling of the global solar corona, *Phys. Plasmas, 6*, 2217.

Munro, R. H. and Jackson, B. V. (1977) Physical-properties of a polar coronal hole from 2 to 5 solar radii, *Astrophys. J., 213*, 874.

Ness, N. F. and Wilcox, J. M. (1965) Sector structure of quiet interplanetary magnetic field, *Science, 148*, 1592.

Neugebauer, M., Forsyth, R. J., Galvin, A. B., Harvey, K. L., Hoeksema, J. T., Lazarus, A. J., Lepping, R. P., Linker, J. A., Mikić, Z., Steinberg, J. T., von Steiger, R., Wang, Y. M., and Wimmer-Schweingruber, R. F. (1998) Spatial structure of the solar wind and comparisons with solar data and models, *J. Geophys. Res., 103* (A7), 14587.

Neugebauer, M., Liewer, P. C., Smith, E. J., Skoug, R. M., and Zurbuchen, T. H. (2002) Sources of the solar wind at solar activity maximum, *J. Geophys. Res., 107* (A12), 1488, doi:10.1029/2001JA000306.

Odstrcil, D., Pizzo, V. J., Linker, J. A., Riley, P., Lionello, R., and Miki´c, Z. (2004) Initial coupling of coronal and heliospheric numerical magnetohydrodynamic codes, *J. Atmos. Sol.-Terr. Phys*., 66, 1311.

Parker, E. N. (1958) Dynamics of the interplanetary gas and magnetic fields, *Astrophys. J., 128*, 664.

Parker, E. N. (1991) Heating Solar Coronal Holes, *Astrophys. J., 372*, 719.

Phillips, J. L., Bame, S. J., Barnes, A., Barraclough, B. L., Feldman, W. C., Goldstein, B. E., Gosling, J. T., Hoogeveen, G. W., McComas, D. J., Neugebauer, M., and Suess, S. T. (1995) Ulysses solar-wind plasma observations from pole to pole, *Geophys. Res. Lett., 22* (23), 3301.

Pneuman, G. W. and Kopp, R. A. (1971) Gas-magnetic field interactions in solar corona, *Sol. Phys., 18*, 258.

Riley, P., Linker, J. A., and Mikić, Z. (2001) An empirically-driven global MHD model of the solar corona and inner heliosphere, *J. Geophys. Res., 106* (A8), 15889.

Roussev, I. I., Gombosi, T. I., Sokolov, I. V., Velli, M., Manchester, W., DeZeeuw, D. L., Liewer, P., Tóth, G., and Luhmann, J. (2003) A three-dimensional model of the solar wind incorporating solar

magnetogram observations, *Astrophys. J., 595*, L57.

Schatten, K. H., Wilcox, J. M., and Ness, N. F. (1969) A model of interplanetary and coronal magnetic fields, *Sol. Phys., 6*, 442.

Schatten, K. H. (1971) Current sheet model of the solar corona, *Cosmic Electrodyn., 2*, 232.

Schunk, R. W. (1977) Mathematical structure of transport equations for multispecies flows, *Rev. Geophys. Space Phys.,* 15, 429.

Siscoe, G. L. (1983) Solar system magnetohydrodynamics, Solar-Terrestrial Physics, Principles and Theoretical Foundations, edited by R. L. Carovillano and J. M. Forbes, pp. 11-100, D. Reidel, Hingham, Mass.

Sittler, E. C. and Guhathakurta, M. (1999) Semiempirical two-dimensional magnetohydrodynamic model of the solar corona and interplanetary medium, *Astrophys. J., 523*, 812.

Steinolfson, R. S., Suess, S. T., and Wu, S. T. (1982) The steady global corona, *Astrophys. J., 255*, 730.

Suess, S. T., Wang, A. H., and Wu, S. T. (1996) Volumetric heating in coronal streamers, *J. Geophys. Res., 101* (A9), 19957.

Suess, S. T., Wang, A. H., Wu, S. T., Poletto, G., and McComas, D. J. (1999) A two-fluid, MHD coronal model, *J. Geophys. Res., 104* (A3), 4697.

Suzuki, T. K. and Inutsuka, S. (2005) Making the corona and the fast solar wind: A self-consistent simulation for the low-frequency alfven waves from the photosphere to 0.3 Au, *Astrophys. J., 632*, L49.

Tanaka, T. (1994) Finite volume TVD scheme on an unstructured grid system for three-dimensional MHD simulation of inhomogeneous systems including strong background potential fields, *J. Comput. Phys., 111*, 381.

Tóth, G., Sokolov, I. V., Gombosi, T. I., Chesney, D. R., Clauer, C. R., DeZeeuw, D. L., Hansen, K. C., Kane, K. J., Manchester, W. B., Oehmke, R. C., Powell, K. G., Ridley, A. J., Roussev, I. I., Stout, Q. F., Volberg, O., Wolf, R. A., Sazykin, S., Chan, A., Yu, B., and Kota, J. (2005) Space Weather Modeling Framework: A new tool for the space science community, *J. Geophys. Res., 110*. A12226, doi:10.1029/2005JA011126.

Usmanov, A. V. (1993a) Interplanetary magnetic-field structure and solar-wind parameters as inferred from solar magnetic-field observations and by using a numerical 2-D MHD model, *Sol. Phys., 143*, 345.

Usmanov, A. V. (1993b) The global structure of the solar-wind in June 1991, *Sol. Phys., 148*, 371.

Usmanov, A. V. and Dryer, M. (1995) A global 3-D simulation of interplanetary dynamics in June 1991, *Sol. Phys., 159*, 347.

Usmanov, A. V., Goldstein, M. L., Besser P., and Fritzer, J. M. (2000) A global MHD solar wind model with WKB Alfven waves: Comparison with Ulysses data, *J. Geophys. Res., 105* (A6), 12675.

Usmanov, A. V. and Goldstein, M. L. (2003) A tilted-dipole MHD model of the solar corona and solar wind, *J. Geophys. Res., 108* (A9), 1354, doi:10.1029/2002JA009777.

Wang, A. H., Wu, S. T., Suess, S. T., and Poletto, G. (1998) Global model of the corona with heat and momentum addition, *J. Geophys. Res., 103* (A2), 1913.

Wang, Y. M. and Sheeley, N. R. (1990) Solar-wind speed and coronal flux-tube expansion, *Astrophys. J., 355*, 726

Washimi, H. and Sakurai, T. (1993) A simulation study of the solar-wind including the solar rotation effect, *Sol. Phys., 143*, 173.

Wilcox Solar Observatory (2008) (http://wso.stanford.edu/).

Withbroe, G. L. (1988) The temperature structure, mass, and energy-flow in the corona and Inner Solar-Wind, *Astrophys. J., 325*, 442.

Zhao, X. P. and Hoeksema, J. T. (1995) Prediction of the interplanetary magnetic-field strength, *J. Geophys. Res., 100* (A1), 19.